DOI: 10.1002/chem.200800817

Nematic and Columnar Ordering of a PEG–Peptide Conjugate in Aqueous Solution

Ian W. Hamley,*[a, d] Marta J. Krysmann,[a] Antonios Kelarakis,[a, e] Valeria Castelletto,[a] Laurence Noirez,[b] Rohan A. Hule,[c] and Darrin J. Pochan[c]

Abstract: The self-assembly in aqueous solution of a PEG–peptide conjugate is studied by spectroscopy, electron microscopy, rheology and small-angle X-ray and neutron scattering (SAXS and SANS). The peptide fragment, FFKLVFF is based on fragment KLVFF of the amyloid β-peptide, Aβ-(16–20), extended by two hydrophobic phenylalanine units. This is conjugated to PEG which confers water solubility and leads to distinct self-assembled structures. Small-angle scattering reveals the formation of cylindrical fibrils comprising a peptide core and PEG corona. This constrained structure leads to a model parallel β-sheet self-assembled structure with a radial arrangement of β sheets. On increasing concentration, successively nematic and hexagonal columnar phases are formed. The flow-induced alignment of both structures was studied in situ by SANS using a Couette cell. Shear-induced alignment is responsible for the shear thinning behaviour observed by dynamic shear rheometry. Incomplete recovery of moduli after cessation of shear is consistent with the observation from SANS of retained orientation in the sample.

Keywords: amphiphiles · liquid crystals · peptides · polymer–peptide conjugates · self-assembly

Introduction

The preparation of block copolymers containing peptide sequences conjugated to synthetic polymers offers the scope to develop novel materials with hierarchical nanoscale ordering and the potential to interface with biological systems. There is now an extensive literature concerning the self-assembly of block copolymers containing synthetic polypeptides (linked either to distinct synthetic polypeptides or to other synthetic polymers),[1–6] although there have been fewer studies on conjugates of biomimetic peptides and synthetic polymers.[7–15] Another class of peptide conjugates are peptide amphiphiles containing a hydrophobic chain (or peptide sequence) linked to a hydrophilic peptide sequence, these also exhibit amphiphilicity.[16–21] The formation of fibrils or vesicles by polymer-peptide hybrid macromolecules is well known.[4,13,15–18,22,23] To the best of our knowledge, lyotropic liquid crystal phase formation has, however, not been reported. Nematic phases have been observed[24] for short de novo designed peptides that form fibrils which self-assemble into a nematic phase at sufficiently high concentration, and also for natural (hen lysozyme) amyloid fibrils.[25] Recently, nematic ordering has been reported for a PEG-peptide amphiphile containing a two-tailed peptide motif attached to a rigid aromatic branch point.[26] This forms tape-like aggregates that show nematic ordering at higher concentration. Chiral nematic (cholesteric) and columnar phases are also known for the synthetic polypeptide, poly(γ-benzyl-L-glutamate), PBLG.[27]

The present paper describes our results on the self-assembly in solution of a PEG-peptide conjugate in which the peptide is a modified fragment of the amyloid β (Aβ) peptide, specifically KLVFF (Aβ16–20) extended by two phenylalanine residues at the N terminus to FFKLVFF. This

[a] Prof. I. W. Hamley, M. J. Krysmann, Dr. A. Kelarakis, Dr. V. Castelletto
Department of Chemistry, University of Reading
Whiteknights, Reading RG6 6AD (UK)
Fax: (+44) 118-378-6331
E-mail: I.W.Hamley@reading.ac.uk

[b] Dr. L. Noirez
CEA-CNRS Laboratoire Léon Brillouin
91191 Gif-sur-Yvette (France)

[c] R. A. Hule, Prof. D. J. Pochan
Dept. Materials Science and Delaware Biotechnology Institute
University of Delaware, Newark DE 19716 (USA)

[d] Prof. I. W. Hamley
Diamond Light Source, Chilton, Didcot
Oxfordshire OX11 0DE (UK)

[e] Dr. A. Kelarakis
Current address: National and Kapodistrian University of Athens
Dept. Chemistry, Physical Chemistry Laboratory
Panepistimiopolis, 157 71 Athens (Greece)

peptide is highly hydrophobic but self assembles into fibrils at low concentration in organic solvents.[28] Conjugation to polyethylene glycol (PEG, $M_w = 3300$, $M_w/M_n = 1.04$) confers water solubility. This conjugate is designed to have enhanced fibrillisation capacity of the peptide domain compared to the KLVFF pentapeptide resulting from an increased hydrophobicity due to the additional F residues, but this is balanced by conjugation to PEG of sufficient molar mass. The resultant conjugate shows very interesting amphiphilic behaviour, forming core–shell fibrils which order into nematic and hexagonal columnar phases successively on increasing concentration. Flow alignment of both structures is observed upon application of low frequency steady shear and studied in detail via small-angle neutron scattering, rheology and polarized optical microscopy experiments.

Experimental Section

Synthesis: The PEGylated conjugate was synthesized by solid phase peptide synthesis using standard FastMoc (Fmoc = 9-fluorenylmethyloxycarbonyl protecting group/HBTU activation) chemistry. FFKLVFF-PEG was synthesized on a 0.25 mmol scale using a fully automated peptide synthesizer (433A Applied Biosystems, United Kingdom) which allowed for direct conductivity monitoring of Fmoc deprotection. A PEGylated TentaGel PAP resin was used, with 0.21 mmol g^{-1} substitution of PEG3000 (nominal molar mass) to provide C-terminal PEGylation upon cleavage from the resin. The crude peptide was purified by reverse phase high performance liquid chromatography (RP-HPLC; Perkin Elmer 200) using a C18 preparative column (Macherey Nagel), for 30 min with flow rates 4 mL min^{-1}. A mobile phase of water with 0.1% TFA and acetonitrile with 0.1% TFA was used. Sample elution was monitored by using a UV/Vis detector operating at 220 nm. Molecular weight was determined by MALDI-TOF (α-cyano-4-hydroxy-cinnamic acid matrix), yielding m/z = 4250 g mol^{-1}, consistent with the PEG $M_w = 3300$ g mol^{-1} and an expected peptide mass = 947.2 g mol^{-1}. Fitting the MALDI-TOF data to a Schulz-Zimm distribuition suggests $M_w/M_n < 1.05$. Analytical RP-HPLC on a Vydac 218TP5414 C18 column yielded a single well-defined peak.[29]

Spectroscopic methods: FTIR spectra in the amide band regions were recorded on a Nicolet FTIR Nexus spectrometer equipped with a DTGS detector. Sample solutions in D_2O (2.5 wt%) were sandwiched between two CaF_2 plate windows (spacer 0.006 mm). Spectra were scanned 64 times over the range of 4000–400 cm^{-1}. Spectral Manager for Windows was used for data acquisition and handling.

Circular dichroism (CD) spectra were recorded on a Chirascan spectropolarimeter (Applied Photophysics, UK). The samples were dissolved in water (0.5 wt%), methanol (0.006 and 0.5 wt%) or 2,2,2-trifluoroethanol, TFE (0.036 and 0.5 wt%) and loaded into a 0.1 mm quartz cover slip cuvette. Spectra were obtained from 200 to 260 nm with a 0.5 nm step, 1 nm bandwidth and 1 s collection time per step at 20 °C, taking five averages.

Polarized optical microscopy: POM was performed using an Olympus CX-41 polarized microscope. A 10 wt% sample was placed in a Linkam shear cell and subjected to steady shear. Images were recorded through crossed polarizers (45° to flow direction). The sample thickness was 110 μm.

Small-angle scattering: Small-angle neutron scattering (SANS and rheo-SANS) was performed on the 2D multidetector PAXY of the Laboratoire Léon Brillouin. Samples were placed in a quartz Couette cell (0.1 mm gap) which was used to apply steady shear.[30] Shear rates are defined as $\dot{\gamma} = \Omega\bar{R}/(R_0 - R_1)$, where Ω is the angular velocity, $\bar{R}$ is the average radius and $R_0 = 19.0$ mm and $R_1 = 19.1$ mm are the inner and outer radii. Shear rates applied were 0.1–4.0 s^{-1}. Measurements were performed at room temperature. Data were obtained with neutrons incident along the shear gradient direction (radial configuration) and along the shear direction (tangential configuration) (see also Figure 9). Two wavelengths of 6 and 12 Å were used. The sample-detector was fixed at 2.5 m. The corresponding q range extends from 0.1 to 2.5 nm^{-1}. The SANS data was corrected for the cell efficiency using an incoherent scatterer. Small-angle X-ray scattering (SAXS) was performed on beamline ID02 at the European Synchrotron Radiation Facility, Grenoble France. Samples were placed in sealed cells (1 mm thickness) between mica windows. The wavelength was $\lambda = 1$ Å, and the sample-detector distance was 2 m. SAXS patterns were collected on a CCD detector.

Cryo transmission electron microscopy: Cryo-TEM, performed at the University of Delaware, is a powerful technique to elucidate the self-assembled structure of amphiphilic molecules in solution.[31] A thin film (≈100 nm) of a 1 wt% sample in water was transferred to a lacey carbon grid, blotted with filter paper and plunged into liquid ethane. All samples were prepared using the environmentally controlled, automated Vitrobot from the FEI Company, Hillsboro, OR. In a typical sample preparation, the sample chamber was maintained at 25 °C and 40–50% relative humidity. Prior to plunging in liquid ethane, the sample was blotted with a filter paper 2–3 times for 1 s. Following vitrification, the samples were transferred to a Gatan cryo-holder pre-cooled to −175 °C, before inserting into the electron microscope. Imaging was carried out in bright field mode at 120 kV in a Technai T12 electron microscope (FEI Company, Hillsboro, OR). During imaging, the temperature of the sample holder was maintained at −175 °C to inhibit sublimation of vitreous water.

Rheology: Rheological properties were determined using a controlled stress TA Instruments AR-2000 rheometer (TA Instruments). For a fluid 5 wt% solution of FFKLVFF-PEG, a Mooney geometry was used. For a gel-like 10 wt% sample, a cone-and-plate geometry (cone diameter 20 mm, angle 1°) was used. Frequency sweeps were performed at 25 °C. Preliminary strain sweeps were performed for each sample in order to define the linear viscoelastic region, thus ensuring that moduli were independent of strain.

Results and Discussion

Secondary structure: FTIR spectra for FFKLVFF-PEG in solution show prominent features in the amide I region consistent with β-sheet structure in the peptide, in particular peaks at 1617 and 1675 cm^{-1} (Figure 1).[32,33] The feature at 1617 cm^{-1} can be assigned to parallel β-sheets, the peak at 1675 cm^{-1} is often assigned to antiparallel β-sheets,[34] although it may also arise from bends or turns.[34,35] or even parallel β-sheets.[32] The peak at 1617 cm^{-1} is slightly red-shifted compared to the canonical value 1625 cm^{-1} for parallel β-sheets,[32,33] however, there is a range of values in the literature[35–37] and our result is within this range. In fact, the model for the fibril structure obtained from SAXS (to be discussed, see Figure 4) indicates that the constraint imposed by terminal PEG chains forming the fibril corona causes the peptide strands to adopt a parallel configuration in FFKLVFF-PEG, with a radial arrangement of the β-sheets. For comparison, Figure 1 also includes and FTIR spectrum for FFKLVFF which has peaks in the same positions as FFKLVFF-PEG, although the relative intensities are different (the 1675 cm^{-1} peak is broader and with a lower peak intensity). There is a shift in peak intensities comparing the data for 2.5 and 5 wt% FFKLVFF-PEG, the 1617 cm^{-1} peak being more intense for the more concentrated solution. This may reflect an increase in β-sheet content, or may result from the formation of a nematic phase at 5 wt% (the 2.5 wt% solution was isotropic).

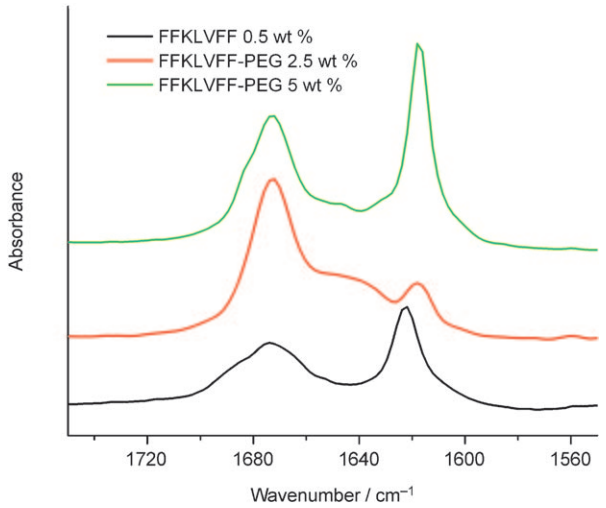

Figure 1. FTIR data for a 2.5 wt% solution of FFKLVFF-PEG in D_2O.

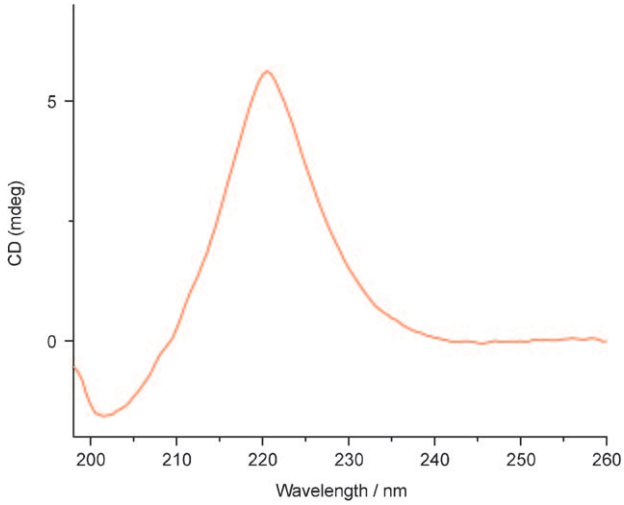

Figure 2. Circular dichroism data for FFKLVFF-PEG in 0.5% aqueous solution.

Circular dichroism (CD) spectra for FFKLVFF-PEG in aqueous (Figure 2) or organic solvents (not shown) in dilute solution do not exhibit characteristics of typical secondary structures, that is, α-helix, β-sheet or random coil. In fact there is a prominent maximum at 220 nm, which is observed consistently, also for lower concentrations. We believe the CD spectrum contains a significant contribution arising from phenylalanine chromophores, since the same maximum is also present in the spectra for FFKLVFF in methanol, as shown in our previous work.[28] A positive CD maximum at 220 nm has also been observed for phenylalanine oligopeptides.[38] It is possible that at the very low concentration used for the CD experiments (attempts to perform CD measurements higher concentration solutions were prohibited by absorption effects), aggregation of FFKLVFF-PEG takes place due to hydrophobic interactions between phenylalanine residues but fully formed β-sheet containing fibrils (as confirmed by FTIR and SAXS, see below, for 2.5 wt% solutions) have not yet developed.

Fibril structure: Cryo-TEM provides direct in situ evidence for fibril formation. The images in Figure 3 were obtained for a 1 wt% aqueous solution and show well-defined fibrils. In some areas, local orientation of fibrils was observed (Figure 3b), possibly a precursor of nematic ordering (see below). The average fibril diameter (from more than 100 fibrils) was (8.4±0.8) nm.

Small-angle X-ray scattering also provided direct evidence for fibril formation in solution. Figure 4 presents SAXS data obtained for a 2.5 wt% aqueous solution, along with a model form factor fit that is based on a core–shell fibril structure as also illustrated in Figure 4. Cryo-TEM indicates that the fibrils have an extremely long persistence length (> 1 μm) and the model SAXS data is therefore based on infinite core–shell cylinders. The SAXS model was constructed as follows: The intensity for a diluted solution of fibrillar objects can be expressed as

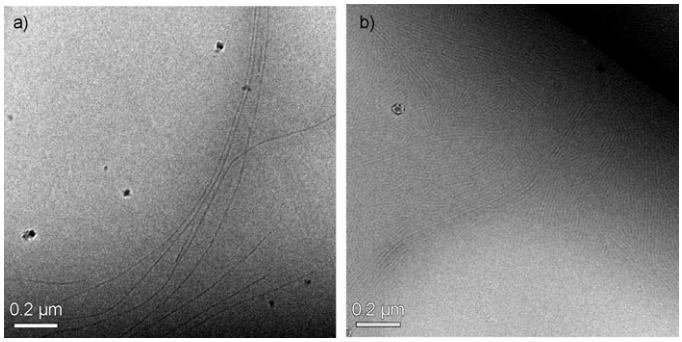

Figure 3. Cryo-TEM images showing well defined fibrils with a persistence length of several microns. a) Isolated fibrils. b) Region with local alignment of fibrils on right-hand side.

$$I(q) = P(q) + \mathrm{BG} \tag{1}$$

where $P(q)$ is the form factor and BG denotes background. The form factor used in our model was that for randomly oriented infinite core–shell cylinders with polydispersity in the external radius of the shell:

$$P(q)\alpha\frac{1}{q^3}\int_0^\infty [(\eta_{\mathrm{core}}-\eta_{\mathrm{corona}})R^2J_1(qR) + (\eta_{\mathrm{solv}}-\eta_{\mathrm{corona}})\chi^2J_1(qx)]^2\exp[-\frac{(\chi-R')^2}{2\sigma^2}]\mathrm{d}x \tag{2}$$

Here R corresponds to the radius of the internal cross section, while $(R'-R)$ is the thickness of the external shell. The parameters η_{core}, η_{corona} and η_{solv} correspond to the electron density of the core, shell and solvent respectively. The term BG in Equation (1) is the background, given by

$$\mathrm{BG} = A + B/q^{\mathrm{C}} \tag{3}$$

We can only determine relative values for $(\eta_{core}-\eta_{corona})$, $(\eta_{solv}-\eta_{corona})$, A and B. Therefore, only the parameters R, R', σ and C are relevant to our fitting. Our results provided $R=2.5$ nm, $R'=2.5$ nm, $\sigma=1$ nm (polydispersity in $R'=20\%$) and $C=-1.3$ (very close to $C=-1$, expected for cylinders). The corresponding dimensions are sketched in Figure 4. The radii of the core–shell fibril structure of our

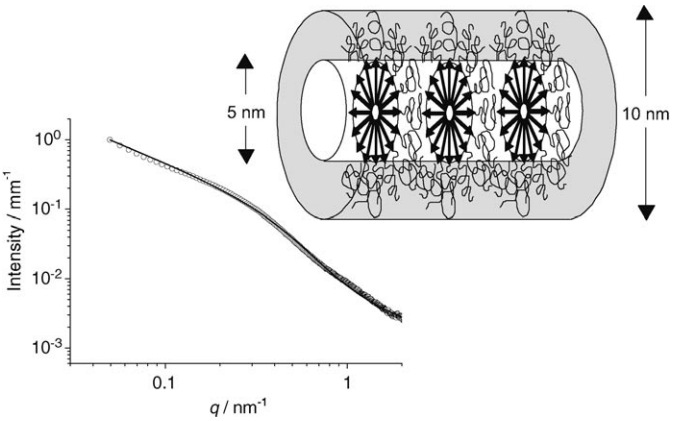

Figure 4. Small-angle X-ray scattering profile for FFKLVFF-PEG (2.5 wt% in D_2O). The solid line is a fit to the form factor of a core–shell cylinder, model shown.

conjugate are consistent with an extended peptide conformation (7×0.35 nm $=2.5$ nm for a β-strand) and a slightly extended coil for the PEG chain ($R_g=1.98$ nm for a PEG Gaussian chain with $M_n=3300$ g mol^{-1}). The total fibril diameter obtained from the SAXS model is (10 ± 2) nm, in excellent agreement with the value from cryo-TEM (which indeed was performed subsequent to our SAXS modelling, providing confidence in the fibril dimensions we had determined). AFM images for dried films of the same sample have been reported elsewhere,[39] the average height of the fibrils is (4.6 ± 0.9) nm, in reasonable agreement with the dimensions from SAXS and cryo-TEM, considering possible artifacts from drying in the AFM film preparation.

As shown in Figure 4, the model of core–shell fibrils with a circular cross-section fits the SAXS data extremely well. It is possible that the aggregates may not have a circular cross-section but may be more tape-like due to preferential staking of hydrophobic faces on the β-sheets. This cannot be resolved from the SAXS data analysis. Börner and co-workers have reported tape-like fibril structures for a PEG-peptide amphiphile comprising a two-tailed peptide motif attached to a rigid branch point.[26] However, in that case the constrained conformation of the molecule favours a planar conformation and hence self-assembly into flattened tapes. In our case, there is no such driving force. Cryo-TEM images show no evidence for tape-like structures (e.g. coexistence of edge-on and side-on morphologies) and nor was this seen by AFM.[39]

Liquid crystal phase behaviour and flow alignment: Increasing the concentration of FFKLVFF-PEG in water to 5 wt%, a nematic phase was observed. Imaging the fluid sample through crossed polarizers (Figure 5) indicates birefringence consistent with a nematic phase. A Schlieren texture is observed in the polarized optical microscope (image not shown), again consistent with a nematic phase. The formation of a nematic phase results from increased packing of fibrils at higher concentration, and increased inter-fibrillar interactions. Since the fibrils are extremely elongated (as evident from cryo-TEM), we believe they can be described as highly anisotropic and interacting semiflexible chains. Models that describe nematic and hexagonal phase formation by such chains have been developed,[40,41] based on repulsive excluded volume interactions and these can account for nematic phase formation at relatively low concentrations. The PEG coronas around the peptide fibrils will mediate the purely repulsive interactions since attractive interactions can result from interpenetration of coronal chains.

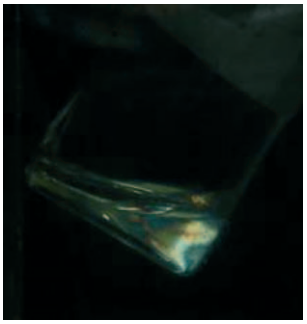

Figure 5. FFKLVFF-PEG (5 wt% in D_2O) in a vial imaged between crossed polarizers exhibits birefringence in the fluid sample.

SANS and SAXS confirmed the formation of a nematic phase, and its alignment under flow. A 5 wt% sample of FFKLVFF-PEG in D_2O was subjected to steady shear in a Couette cell. Figure 6 shows SANS data obtained in the radial configuration obtained in situ before, during and after shear. Before shear, the SANS pattern is isotropic indicating no sample orientation, however, when the sample is under flow, the SANS pattern becomes anisotropic (elliptical), indicating orientation of the fibrils. The extent of orientation increased with shear rate (varied from $\dot{\gamma}=0.1$–4 s^{-1}), however loss of sample was observed at higher shear rates as it was expelled from the Couette cell. Following shear, retention of an aligned SANS pattern was observed. In the tangential direction (data not shown) weak anisotropic scattering was observed, as expected given the uniaxial symmetry of a shear-aligning nematic phase.

Flow-induced birefringence was observed for a sample containing 10 wt% FFKLVFF-PEG (Figure 7). The texture is quite distinct from that observed for the nematic phase at 5 wt%. In fact, a columnar phase is formed at this concentration (and also 15 wt% FFKLVFF-PEG) as confirmed by SAXS and SANS. Figure 7 shows polarized optical micro-

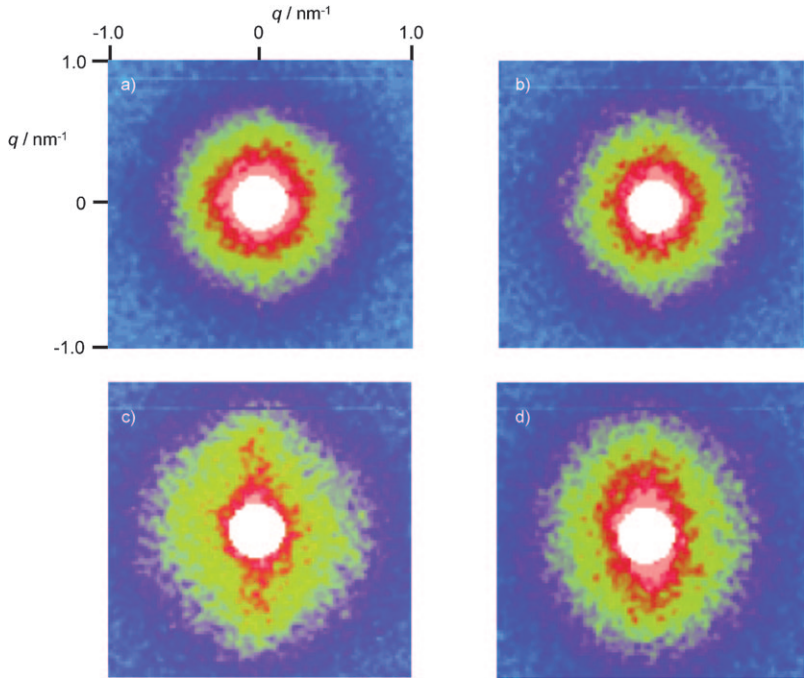

Figure 6. SANS under flow at different shear rates for 5 wt% FFKLVFF-PEG. a) At rest prior to shearing. b) $\dot{\gamma}=0.2\ s^{-1}$. c) $\dot{\gamma}=0.5\ s^{-1}$. d) At rest, following shear. The horizontal axis is the flow velocity direction, the vertical axis is the neutral direction.

scope images of the texture of 10 wt% FFKLVFF-PEG at rest and under flow at $\dot{\gamma}=5\ s^{-1}$. Streaming birefringence was observed under flow, consistent with a shear-aligning columnar phase.[42]

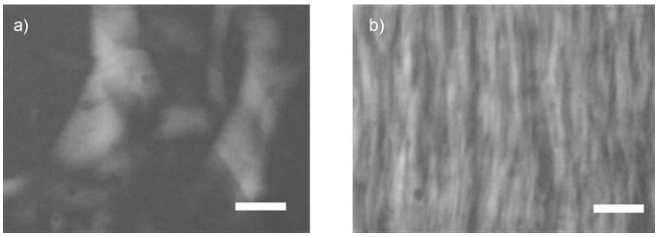

Figure 7. Polarized optical microscopy images of texture of flowing columnar phase (10 wt% sample) a) at rest and b) under flow at $5\ s^{-1}$. The scale bars indicate 100 μm.

Small-angle X-ray scattering on a spontaneously aligned sample confirms that 10 wt% FFKLVFF-PEG forms a hexagonal columnar phase (Figure 8). The hexagonal symmetry is confirmed by the presence of Bragg peaks in the positional ratio $1:\sqrt{3}:\sqrt{4}:\sqrt{7}$. The formation of a hexagonal columnar phase at a higher concentration than that of the nematic phase is consistent with the phase diagrams calculated for extended semiflexible chains, based on repulsive inter-particle interactions.[40,41] The primary peak position $q^*=0.37\ nm^{-1}$ indicates a hexagonal lattice parameter $d=17$ nm.

Small-angle neutron scattering provided further clear evidence for the formation of a columnar structure via a study of shear-induced alignment in a 15 wt% sample of FFKLVFF-PEG in D_2O. The sample was subjected to steady shear in a Couette cell at several shear rates. Figure 9 presents the SANS profiles for a sample under shear at $\dot{\gamma}=1\ s^{-1}$ in radial and tangential directions with respect to the Couette cell, as illustrated. The two-fold symmetry in the SANS pattern obtained with the neutron beam along the radial direction combined with isotropic symmetry in the SANS pattern with the beam along the tangential direction indicate flow-alignment of a cylindrical structure along the velocity direction, as shown. The presence of weak higher order reflections along the meridian in the radial SANS pattern (peak positions in the ratio $1:\sqrt{3}$) is consistent with local hexagonal ordering of the cylinders.

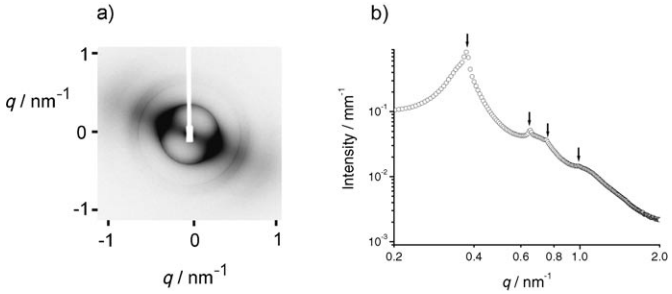

Figure 8. SAXS data for a 10 wt% aqueous solution of FFKLVFF-PEG a) Two-dimensional SAXS pattern showing spontaneous orientation in a liquid cell (perpendicular to X-ray beam direction). b) One-dimensional SAXS profile showing multiple Bragg reflections. The arrows indicate peak positions expected for a hexagonal structure.

Controlled stress rheometry experiments provide confirmation of the change in order of the sample from nematic phase at 5 wt% FFKLVFF-PEG to columnar phase at 10 wt% FFKLVFF-PEG. Figure 10 shows frequency sweeps of dynamic shear moduli G′ and G″ for the two samples. The low frequency response for (both moduli) for the 5 wt% sample is fluid-like. In contrast, for the 10 wt% sample G′ is significantly greater than G″ and both moduli are almost frequency independent. This is consistent with pseudo solid-like behaviour. Shear thinning is observed for both samples following steady shear at a controlled stress for one minute. There is subsequent recovery of the moduli,

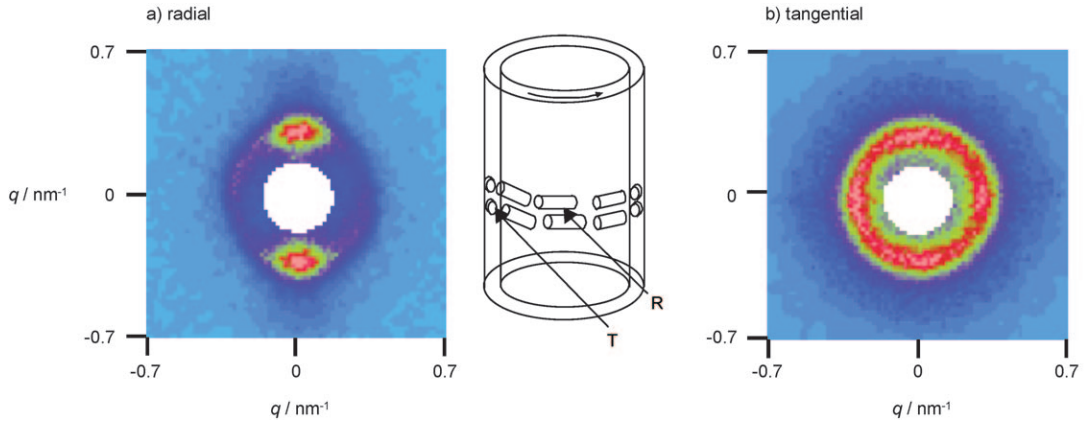

Figure 9. SANS patterns for a 15 wt% solution of FFKLVFF-PEG under steady shear in a Couette cell at $\dot{\gamma}=1\ s^{-1}$. The two configurations of the scattering experiment are illustrated in the central part.

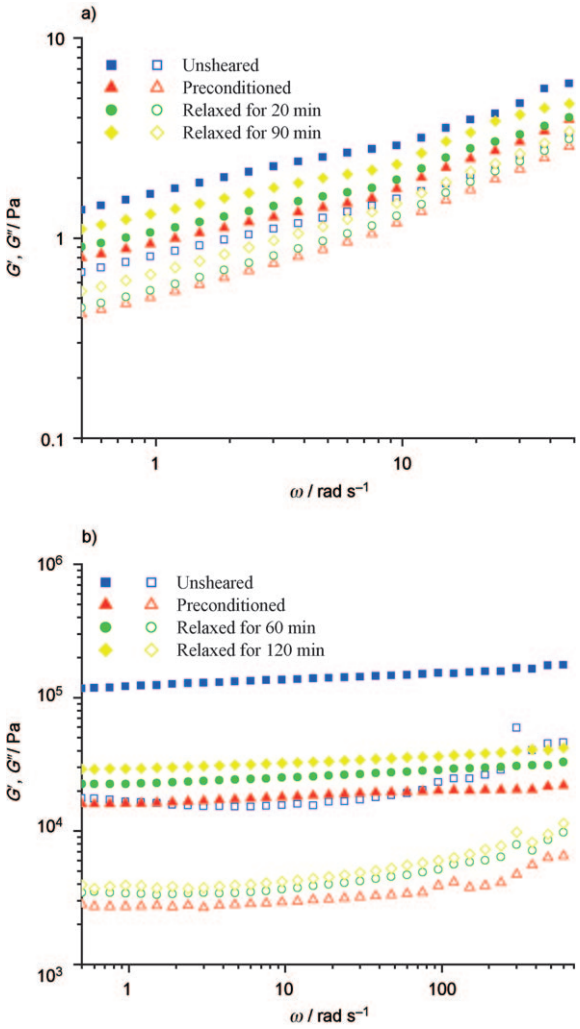

Figure 10. Frequency dependence of dynamic shear moduli for solutions of FFKLVFF-PEG a) 5 wt% sample. Subjected to preconditioning steady shear at $\sigma=50$ Pa for 1 min; b) 10 wt% sample. Subjected to preconditioning steady shear at $\sigma=400$ Pa for 1 min. The solid symbols denote G′, the open ones G″.

although not to their initial values. The shear thinning behaviour followed by partial recovery of moduli is the result of flow-induced alignment of the samples, as confirmed by SANS (Figures 6 and 9).

Summary

The peptide/polymer conjugate FFKLVFF-PEG forms core–shell fibrils in aqueous solution with a core comprising the hydrophobic peptide in an extended β-strand configuration and a shell of hydrophilic PEG. These anisotropic nano-objects self-assemble into lyotropic liquid crystal phases: first nematic, and then hexagonal columnar phases on increasing concentration. The formation of such structures has been rationalized theoretically on the basis of excluded volume packing interactions, however, the presence of PEG in our fibrils presumably modifies the inter-particle interaction such that there is an attractive contribution from the interpenetration and hydration of PEG chains. The flow alignment properties of these phases have been investigated, both nematic and columnar phases were observed to align spontaneously under flow upon loading into cuvettes. A systematic study of shear-induced orientation is presented in this paper, using in situ SANS with a Couette cell geometry. The nematic and columnar phases align progressively better with increasing shear rate up to $\dot{\gamma}=1\ s^{-1}$, above which flow-induced instabilities were noted. Retention of orientation was observed after cessation of shear. This was consistent with rheology data which indicate shear thinning behaviour for both viscous nematic and gel-like columnar phases. However, complete recovery of moduli after shearing was not observed, an effect ascribed to flow-induced orientation. A complete mapping of the phase diagram of the hybrid amphiphilic molecule FFKLVFF-PEG may help to elucidate the nature of the inter-particle interactions, and to facilitate comparison with the related phase behaviour of biomolecules such as DNA (which exhibits chiral nematic and columnar phases[43]) and PBLG. Our observation of nematic

and hexagonal columnar phase formation is fascinating and points to the unique self-assembly properties of these polymer/peptide hybrids.

Acknowledgement

We are grateful to Dr. T. Narayanan (ESRF, Grenoble, France) for assistance with SAXS experiments.

[1] J. J. L. M. Cornelissen, M. Fischer, N. A. J. M. Sommerdijk, R. J. M. Nolte, *Science* **1998**, *280*, 1427.
[2] F. Chécot, S. Lecommandoux, Y. Gnanou, H.-A. Klok, *Angew. Chem.* **2002**, *114*, 1395; *Angew. Chem. Int. Ed.* **2002**, *41*, 1340.
[3] F. Chécot, S. Lecommandoux, H.-A. Klok, Y. Gnanou, *Euro. Phys. J. E* **2003**, *10*, 25.
[4] H.-A. Klok, *J. Polym. Sci. Part A* **2004**, *43*, 1.
[5] H. Iatrou, H. Frielinghaus, S. Hanski, N. Ferderigos, J. Ruokolainen, O. Ikkala, D. Richter, J. Mays, N. Hadjichristidis, *Biomacromolecules* **2007**, *8*, 2173.
[6] R. Sigel, M. Losik, H. Schlaad, *Langmuir* **2007**, *23*, 7196.
[7] T. S. Burkoth, T. L. S. Benzinger, D. N. M. Jones, K. Hallenga, S. C. Meredith, D. G. Lynn, *J. Am. Chem. Soc.* **1998**, *120*, 7655.
[8] T. S. Burkoth, T. L. S. Benzinger, V. Urban, D. G. Lynn, S. C. Meredith, P. Thiyagarajan, *J. Am. Chem. Soc.* **1999**, *121*, 7429.
[9] P. Thiyagarajan, T. S. Burkoth, V. Urban, S. Seifert, T. L. S. Benzinger, D. M. Morgan, D. Gordon, S. C. Meredith, D. G. Lynn, *J. Appl. Crystallogr.* **2000**, *33*, 535.
[10] G. W. M. Vandermeulen, C. Tziatzios, H.-A. Klok, *Macromolecules* **2003**, *36*, 4107.
[11] I. W. Hamley, I. A. Ansari, V. Castelletto, H. Nuhn, A. Rösler, H.-A. Klok, *Biomacromolecules* **2005**, *6*, 1310.
[12] H.-A. Klok, G. W. M. Vandermeulen, H. Nuhn, A. Rösler, I. W. Hamley, V. Castelletto, H. Xu, S. Sheiko, *Faraday Discuss.* **2005**, *128*, 29.
[13] D. W. P. M. Löwik, L. Ayres, J. M. Smeenk, J. C. M. van Hest, *Adv. Polym. Sci.* **2006**, *202*, 19.
[14] J. C. M. Van Hest, *J. Macromol. Sci. Polym. Rev.* **2007**, *47*, 63.
[15] H. G. Börner, H. Schlaad, *Soft Matter* **2007**, *3*, 394.
[16] J. D. Hartgerink, E. Beniash, S. I. Stupp, *Science* **2001**, *294*, 1684.
[17] J. D. Hartgerink, E. Beniash, S. I. Stupp, *Proc. Natl. Acad. Sci. USA* **2002**, *99*, 5133.
[18] K. L. Niece, J. D. Hartgerink, J. J. J. M. Donners, S. I. Stupp, *J. Am. Chem. Soc.* **2003**, *125*, 7146.
[19] S. Santoso, W. Hwang, H. Hartman, S. Zhang, *Nano Lett.* **2002**, *2*, 687.
[20] X. Zhao, S. Zhang, *Trends Biotechnol.* **2004**, *22*, 470.
[21] D. W. P. M. Löwik, J. Garcia-Hartjes, J. T. Meijer, J. C. M. van Hest, *Langmuir* **2005**, *21*, 524.
[22] S. Vauthey, S. Santoso, H. Gong, N. Watson, S. Zhang, *Proc. Natl. Acad. Sci. USA* **2002**, *99*, 5355.
[23] I. W. Hamley, *Angew. Chem.* **2007**, *119*, 8274; *Angew. Chem. Int. Ed.* **2007**, *46*, 8128.
[24] A. Aggeli, I. A. Nyrkova, M. Bell, R. Harding, L. Carrick, T. C. B. McLeish, A. N. Semenov, N. Boden, *Proc. Natl. Acad. Sci. USA* **2001**, *98*, 11857.
[25] A. M. Corrigan, C. Müller, M. R. H. Krebs, *J. Am. Chem. Soc.* **2006**, *128*, 14740.
[26] H. G. Börner, B. Smarsly, J. Hentschel, A. Rank, R. Schubert, Y. Geng, D. E. Discher, T. Hellweg, A. Brandt, *Macromolecules* **2008**, *41*, 1430.
[27] V. Luzzati, M. Cesari, G. Spach, F. Masson, B. Vincent, *J. Mol. Biol.* **1961**, *3*, 566.
[28] M. J. Krysmann, V. Castelletto, I. W. Hamley *Soft Matter* **2007**, *3*, 1401.
[29] I. W. Hamley, M. J. Krysmann, *Langmuir* **2008**, in press.
[30] P. Baroni, C. Pujolle, L. Noirez, *Rev. Sci. Instrum.* **2001**, *72*, 2686.
[31] H. Cui, T. K. Hodgdon, E. W. Kaler, L. Abezgaous, D. Danino, M. Lubovsky, Y. Talmon, D. J. Pochan, *Soft Matter* **2007**, *3*, 945.
[32] H. Susi, D. M. Byler, *Arch. Biochem. Biophys.* **1987**, *258*, 465.
[33] A. Barth, C. Zscherp, *Q. Rev. Biophys.* **2002**, *35*, 369.
[34] J. T. Pelton, L. R. McLean, *Anal. Biochem.* **2000**, *277*, 167.
[35] B. Stuart, *Biological Applications of Infrared Spectroscopy*, Wiley, Chichester, **1997**.
[36] W. K. Surewicz, H. H. Mantsch, *Biochim. Biophys. Acta* **1988**, *952*, 115.
[37] P. Haris, D. Chapman, *Biopolymers* **1995**, *37*, 251.
[38] E. Peggion, M. Palumbo, G. M. Bonora, C. Toniolo, *Bioorg. Chem.* **1974**, *3*, 125.
[39] M. J. Krysmann, I. W. Hamley, S. S. Funari, E. Canetta, *Macromol. Chem. Phys.* **2008**, *209*, 883.
[40] R. Hentschke, J. Herzfeld, *Phys. Rev. A* **1991**, *44*, 1148.
[41] J. V. Selinger, R. F. Bruinsma, *Phys. Rev. A* **1991**, *43*, 2922.
[42] M. Impéror-Clerc, I. W. Hamley, P. Davidson, *Macromolecules* **2001**, *34*, 3503.
[43] F. Livolant, A. Leforestier, *Prog. Polym. Sci.* **1996**, *21*, 1115.

Received: April 30, 2008
Published online: July 10, 2008

